Journal of Hazardous Materials 180 (2010) 735–740

Contents lists available at ScienceDirect

Journal of Hazardous Materials

journal homepage: www.elsevier.com/locate/jhazmat

# Preparation, characterization and activity evaluation of heterostructure $In_2O_3/In(OH)_3$ photocatalyst

Chen Shifu*, Yu Xiaoling, Zhang Huaye, Liu Wei

*Department of Chemistry, Huaibei Normal University, Anhui, Huaibei 235000, People's Republic of China*

ARTICLE INFO

*Article history:*
Received 19 January 2010
Received in revised form 10 April 2010
Accepted 27 April 2010
Available online 2 May 2010

*Keywords:*
Heterostructure
$In_2O_3/In(OH)_3$
Synthesis
Activity
Characterization

ABSTRACT

In this paper, the heterostructure $In_2O_3/In(OH)_3$ photocatalyst was prepared by programmed thermal treatment of $In(OH)_3$ using $In(NO_3)_3{\cdot}9H_2O$ as the precursor. Various characterization methods such as X-ray power diffraction (XRD), UV–vis diffuse reflectance spectroscopy (DRS), Fourier transform infrared spectrometry (FT-IR) and transmission electron microscopy (TEM) were employed to investigate the structure, morphologies, and optical properties. Terephthalic acid was used as a probe molecule to detect the generation of hydroxyl radicals (•OH) on the surface of UV-illuminated photocatalyst by a photoluminescence (PL) technique. The results showed that the photocatalytic activity of the heterostructure $In_2O_3/In(OH)_3$ was higher than that of single $In_2O_3$ or $In(OH)_3$. The increased photocatalytic activity may be attributed to the formation of the heterojunction between $In_2O_3$ and $In(OH)_3$, which suppresses the recombination of photoexcited electrons–hole pairs.



## 1. Introduction

Nanoparticles with a uniform size and shape have attracted much attention because of their technological and fundamental scientific importance, novel physical properties and potential applications in the areas such as optoelectronics, information storage, catalysis, and biosensors [1,2]. The methods to control the synthesis of such nanoparticles have been extensively investigated [3–5]. As an n-type semiconductor oxide, indium oxide ($In_2O_3$) has been used widely as ultra-sensitive toxic gas detectors, transparent conductors, solar cells, flat panel displays, and other optoelectronic devices etc. [6–10]. Generally speaking, $In_2O_3$ can be obtained through the calcination of $In(OH)_3$, which is prepared by hydrolysis of indium nitrate or other indium salts in NaOH aqueous solution or ammonia solution. Meanwhile, it is known that $In(OH)_3$ is a wide-gap semiconductor material with a direct band gap of 5.15 eV and deep absorption in UV region [11]. As the photocatalysts, the preparation method, photocatalytic activity and electrochemical property of single $In(OH)_3$ or $In_2O_3$ has been widely investigated. Wang and co-workers successfully synthesized the monodisperse single-crystalline $In(OH)_3$ nanotubes and found it exhibited highly photocatalytic activity through the benzene removal [12]. Sulfur-substituted and zinc-doped $In(OH)_3$ were synthesized and their photoactivity for $H_2$ production under visible light illumination was also investigated [13].

Heterostructure semiconductor materials as the photocatalysts have become a highlight in recent years. It would be a beneficial solution for the disadvantages of the single photocatalyst such as rapid recombination of photogenerated carriers and the relative narrow spectrum response. Composite photocatalysts, such as $ZnO/TiO_2$ [14], $SnO_2/ZnO$, $SnO_2/TiO_2$, $WO_3/TiO_2$ [15], $NiO/TiO_2$ [16], $CuBi_2O_4/TiO_2$ [17], $ZnO/In_2O_3$ [18] etc. have been investigated extensively. The results showed that nearly all the composite semiconductors had higher photocatalytic activity than single ones. However, to the best of our knowledge, the synthesis and optical properties of the heterostructure $In_2O_3/In(OH)_3$ photocatalyst have never been reported. Herein, we reported the preparation of the $In(OH)_3/In_2O_3$ photocatalyst. The structure, morphologies, and optical properties of the $In_2O_3/In(OH)_3$ were characterized by X-ray power diffraction (XRD), UV–vis diffuse reflectance spectroscopy (DRS), Fourier transform infrared spectrometry (FT-IR), and transmission electron microscopy (TEM). Rhodamine B was selected as a model substrate to evaluate the photocatalytic activity of the samples under UV-illumination. The possible mechanism was also investigated.

## 2. Experimental

### 2.1. Materials

Indium nitrate ($In(NO_3)_3$) was used as the In source. Ammonia solution ($NH_4OH$), terephthalic acid ($C_8H_6O_4$), sodium hydroxide (NaOH), rhodamine B (RhB) and other chemicals used in the experiments were of analytically pure grade. They were purchased from

* Corresponding author. Tel.: +86 561 3806611; fax: +86 561 3803141.
*E-mail address:* chshifu@hbcnc.edu.cn (C. Shifu).

0304-3894/$ – see front matter © 2010 Elsevier B.V. All rights reserved.
doi:10.1016/j.jhazmat.2010.04.108

Shanghai Sinopharm Chemical Reagent Co., Ltd. Deionized water was used throughout the experiment.

### 2.2. Preparation of heterostructure $In(OH)_3/In_2O_3$

Heterostructure $In(OH)_3/In_2O_3$ was prepared through programmed thermal treatment of $In(OH)_3$ precursor. $In(OH)_3$ precursor was produced via the precipitation of indium nitrate in ammonia solution.

The synthesis reactions can be expressed as:

$$In(NO_3)_3 + NH_4OH \rightarrow In(OH)_3\downarrow + NH_4NO_3 \quad (1)$$

$$In(OH)_3 \rightarrow In_2O_3 + H_2O \quad (2)$$

The detailed preparation procedure was depicted as follows.

A 12% aqueous solution $NH_4OH$ was added dropwise to an aqueous $In(NO_3)_3$ solution (0.5 M) under continuous stirring until the final pH of the solution was 8.0. The resulted white precipitate was washed thoroughly with distilled water using centrifugation. After the filtration, the obtained white precipitate $In(OH)_3$ was dried at 120 °C for 12 h. The obtained sample was firstly kept at 200 °C for 2 h, followed by thermal treatment at 240 °C for appropriate time. The heterostructure $In_2O_3/In(OH)_3$ samples with different composition ratio were prepared.

### 2.3. Characterization

In order to determine the crystal phase composition, X-ray diffraction (XRD) measurement was carried out at room temperature using a DX-2000 X-ray powder diffractometer with Cu Kα radiation and a scanning speed of 3°/min. The accelerating voltage and emission current were 40 kV and 30 mA, respectively. Composition quantitative analysis of the sample was performed on multi-phase patterns easily by means of reference intensity ratios (i.e., RIR, also called $I/I_c$ in the PDF database). When the sample is consisted of two phases (a and b), the RIR value could be read from the PDF database, and the weight ratio of each composition can be calculated using the following formula:

$$W_a = \frac{I_a}{I_a + (I_b/(RIR_b/RIR_a))} \quad (3)$$

$$W_b = \frac{I_b}{I_b + (I_a/(RIR_a/RIR_b))} = 1 - W \quad (4)$$

where $I_a$ and $I_b$ are integrated intensities of the strongest peak of phase a and phase b, respectively.

In order to investigate the optical and photochemical properties of the samples, UV–vis diffuse reflectance spectroscopy measurements were carried out using a Hitachi UV-365 spectrophotometer equipped with an integrating sphere attachment. The analysis range was from 230 nm to 650 nm, and $BaSO_4$ was used as a reflectance standard. The infrared absorption spectra were recorded over the frequency range from 400 $cm^{-1}$ to 4000 $cm^{-1}$ using a Nicolet 6700 FT-IR spectrophotometer (USA). The spectra were measured after the spectrum scan of the blank pure KBr pellet.

Transmission electron microscopy (TEM), high-resolution transmission electron microscopy (HRTEM) images and selected area electron diffraction (SAED) were performed with a JEOL-2010 transmission electron microscope, using an accelerating voltage of 200 kV.

### 2.4. Evaluation of photocatalytic activity

The experiments were carried out in a photoreaction apparatus. RhB was selected as a model of dye pollutant to evaluate the photooxidation activity of the samples. The amount of photocatalyst used in the experiments was 2.0 g $L^{-1}$, and the initial concentration of RhB was $5.0 \times 10^{-6}$ mol $L^{-1}$. A schematic of the photoreactor and the detailed procedure were shown in Refs. [15,16].

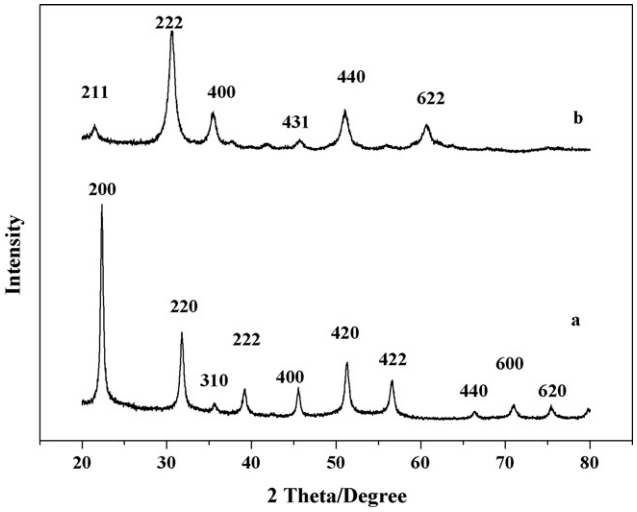


**Fig. 1.** XRD patterns of $In(OH)_3$ (a) and $In_2O_3$ (b).

### 2.5. Analysis

The concentration of rhodamine B in solution was determined spectrophotometrically. The photodegradation efficiency of rhodamine B was calculated from the following expression:

$$\eta = \frac{C_0 - C_t}{C_0} \times 100\%$$

where $\eta$ is the photocatalytic efficiency; $C_0$ is the concentration of reactant before illumination; $C_t$ is the concentration of reactant after illumination time t.

Photoluminescence (PL) technique with terephthalic acid as a probe molecule was used to detect the formation of free •OH radicals on the surface of the UV-illuminated photocatalyst. Terephthalic acid readily reacts with •OH to produce highly fluorescent product, 2-hydroxyterephthalic acid [19]. The detailed experimental procedure is given in Ref. [20].

## 3. Results and discussion

The XRD patterns of $In(OH)_3$ and $In_2O_3$ are shown in Fig. 1. $In(OH)_3$ was prepared by calcination of precursor at 200 °C for 2 h. $In_2O_3$ was produced from $In(OH)_3$ precursor through direct thermal treatment at 240 °C for 6 h. The diffraction peaks are in agreement with that reported in the JCPDS database card (No. 89-4595 and No. 85-1338). Fig. 1a shows a well-defined peak at $2\theta = 22.26°$, corresponding to the (2 0 0) plane of $In(OH)_3$, the peaks at $2\theta = 51.16°$ and 56.46° assigned to the (4 2 0) and (4 2 2) planes, respectively. From Fig. 1b, it is known that the diffraction peaks at $2\theta = 21.53°$, 30.65°, 51.07°, 60.70° are consistent with the (2 1 1), (2 2 2), (4 4 0), and (6 2 2) reflections of $In_2O_3$, respectively.

Fig. 2 shows the XRD patterns of the heterostructure $In_2O_3/In(OH)_3$ with different composition ratios of $In(OH)_3$ and $In_2O_3$. Sample (a) was obtained via heat treatment of $In(OH)_3$ precursor at 200 °C for 2 h, and samples (b–e) were prepared by further heat treatment of the sample (a) at 240 °C for 2 h, 3 h, 5 h and 8 h, respectively. From Fig. 2, it is clear that the samples a and e show a pure phase of $In(OH)_3$ and $In_2O_3$, respectively. As for the sample b, the dominant component was $In(OH)_3$, and $In_2O_3$ was not detected. The possible reason is that the amount of $In_2O_3$ is so small that the equipment does not detect its existence. From Fig. 2, it can be seen that, with the increase in the heat treatment time, $In(OH)_3$ will be

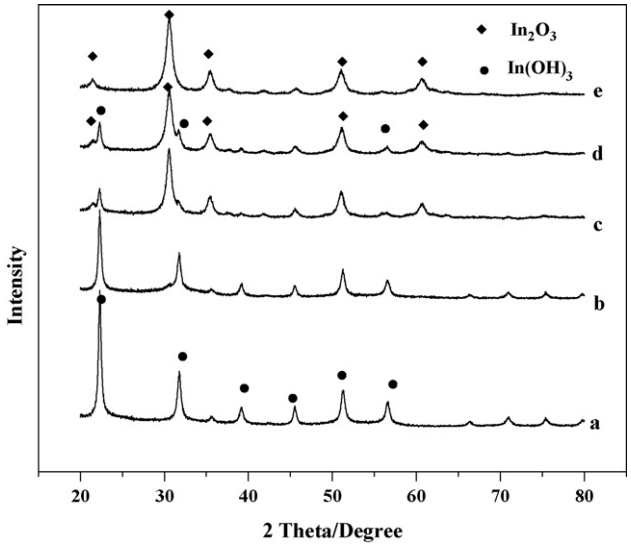


**Fig. 2.** XRD patterns of the samples. (a) $In(OH)_3$; (b–d) heterostructure $In_2O_3/In(OH)_3$; (e) $In_2O_3$.

transformed into $In_2O_3$ gradually. Under heat treatment at 240 °C for 3 h and 5 h, the samples c and d consist of $In(OH)_3$ and $In_2O_3$, and $In_2O_3$ becomes the dominant component in the samples. When the sample was heat treated at 240 °C for 8 h, $In(OH)_3$ was totally transformed to $In_2O_3$, as is shown in Fig. 2e.

Composition quantitative analysis was performed using the Eqs. (3) and (4) by means of RIR quantitative analysis. After identifying the phases in the scan pattern using MDI Jade software, the RIR values of $In(OH)_3$ (RIR = 11.2) and $In_2O_3$ (RIR = 13.22) can be read from the matching PDF card database. The result of composition quantitative analysis of the heterostructure $In_2O_3/In(OH)_3$ samples is shown in Table 1. From Table 1, it is clear that the result is consistent with the analysis of Fig. 2.

To know the specific procedure of the transformation from $In(OH)_3$ to $In_2O_3$, temperature-dependent X-ray diffraction measurement was carried out. The programmed heating temperature of the $In(OH)_3$ precursor was fixed in the range of 100–300 °C, and the rate of the temperature increase is 5 °C/min. The XRD patterns were recorded at intervals of every 10 °C. For briefness, we only presented the XRD patterns recorded in the range of 180–250 °C.

As can be seen in Fig. 3, the characteristic peak at $2\theta = 22.26°$ of $In(OH)_3$ becomes weak with the increase in the temperature, while the characteristic peak at $2\theta = 30.65°$ of $In_2O_3$ appears and becomes stronger, indicating that $In(OH)_3$ was transformed to $In_2O_3$ gradually. At 220 °C, the characteristic peaks of $In(OH)_3$ and $In_2O_3$ coexist. It can be inferred that only a fraction of $In(OH)_3$ is transformed into $In_2O_3$. When the temperature reaches 230 °C, $In_2O_3$ becomes the dominant component; and characteristic peaks of $In(OH)_3$ cannot be detected when the temperature is above 240 °C. From the above results, it is clear that there is a litter difference in the transformation temperature of $In(OH)_3$ to $In_2O_3$ between Figs. 2 and 3. It may be attributed to the different equipments.

**Table 1**
Result of quantitative analysis of the samples.

| T sample | Weight ratio (%) | |
|---|---|---|
| | $In(OH)_3$ | $In_2O_3$ |
| a | 100 | 0 |
| b | 96.3 | 3.7 |
| c | 20.2 | 79.8 |
| d | 12.1 | 87.9 |
| e | 0 | 100 |

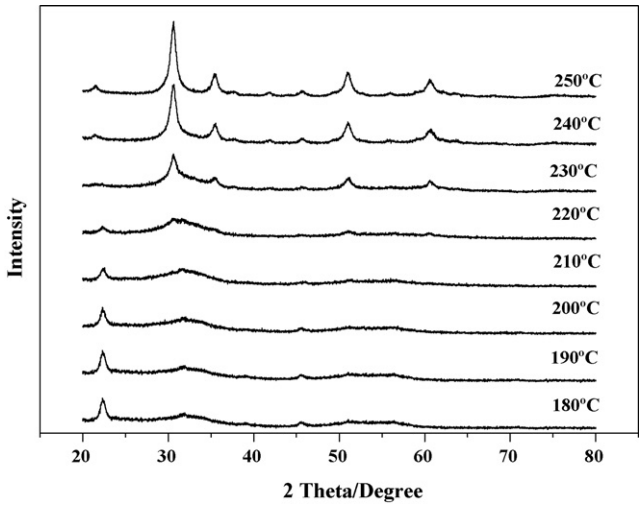


**Fig. 3.** Temperature-dependent XRD patterns of the samples.

The electrochemical properties of single $In(OH)_3$ and $In_2O_3$ have been investigated extensively. Avivi et al. [11] employed DRS as a characterization tool to estimate the optical band gap of $In(OH)_3$. The results showed that, apart from the strong band-gap absorption (5.15 eV), there were two other indirect absorption bands as peaks at 4.24 eV and 4.78 eV; while the reports on the band structure of $In_2O_3$ still remained controversial. A number of researchers reported that $In_2O_3$ was an indirect band-gap semiconductor. The direct band gap determined by the optical absorption data lies in the range between 3.50 eV and 3.75 eV [21–23], and indirect band gap ascribing to the energy exchange between photons and crystal lattice lies in the range between 2.3 eV and 2.8 eV [24,25]. Nevertheless, indirect transition may not necessarily occur. Among the published reports, the band gap of $In_2O_3$ calculated varied from 2.3 eV to 3.57 eV. For example, Sun et al. [26] utilized transformed diffuse reflectance spectra to estimate the band gap of $In_2O_3$, and the plot of the modified Kubelka–Munk function versus the energy of exciting light afforded band-gap energy of 3.2 eV. However, a report released by Walsh et al. [27] indicates that the $In_2O_3$ band gap may actually be as low as 2.9 eV.

In order to study the optical properties of the heterostructure $In_2O_3/In(OH)_3$, the UV–vis DRS characterization is performed, as is shown in Fig. 4. For comparison, the spectra of pure $In(OH)_3$

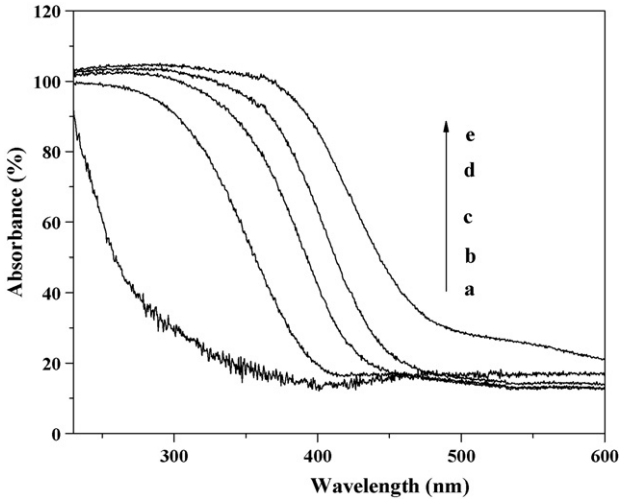


**Fig. 4.** UV–vis diffuse reflection spectra of the samples. (a) $In(OH)_3$; (b–d) heterostructure $In_2O_3/In(OH)_3$; (e) $In_2O_3$.

(a) and $In_2O_3$ (e) synthesized under the same experimental conditions are also plotted. From Fig. 4, it can be seen that the pure $In_2O_3$ and $In(OH)_3$ show a clear absorption edge at around 480 nm (2.58 eV) and 240 nm (5.17 eV), respectively. The heterostructure $In(OH)_3/In_2O_3$ samples exhibit a mixed absorption property of both $In(OH)_3$ and $In_2O_3$. And with the increase in the amount of $In_2O_3$, the absorption wavelength range is extended toward the long wave region.

It is noteworthy that, from the XRD characterization (see Fig. 2), the sample b exhibits a dominate $In(OH)_3$ phase with traces of $In_2O_3$. However, according to the UV–vis diffuse reflectance spectroscopy of the sample, it can be seen that its optical response has a red shift toward the longer wavelength region, compared with the $In(OH)_3$. It proved the existence of $In_2O_3$. The result verified the formation of the heterostructure $In_2O_3/In(OH)_3$. From Fig. 4, it can also be seen that the amount of $In_2O_3$ of the sample increases with the increase in the heat treatment time. The result is the same as the conclusion of the XRD.

FT-IR spectra characterization was carried out to get further information on the material composition and structural characteristic. Typical IR spectra of the $In(OH)_3$ precursor, the heterostructure $In_2O_3/In(OH)_3$ and as-prepared $In_2O_3$ are shown in Fig. 5. From Fig. 5a, it can be seen that the spectrum exhibits the typical characteristic peaks of the deformation vibrations of In–OH groups along with the bands within the wavenumber 750–1200 $cm^{-1}$ region, and it is in accordance with the previous reports [28,29]. For the heterostructure $In_2O_3/In(OH)_3$ photocatalyst (sample b), the appearance of three sharp bands peaking at 540 $cm^{-1}$, 565 $cm^{-1}$ and 600 $cm^{-1}$ can be assigned to the phonon vibrations of In–O bonds [30], which indicates the formation of the cubic $In_2O_3$. Meanwhile, the characteristic absorption band within the wavenumber 750–1200 $cm^{-1}$ region of the In–OH overtly decreased. After $In(OH)_3$ precursor was directly calcined at 240 °C for 6 h, the obtained sample showed the prominent peaks of the cubic $In_2O_3$. The absorption corresponding to the In–OH vibrations decreased to the state of neglect, indicating the total transformation of $In(OH)_3$ into $In_2O_3$. Besides, no impurity or solvent residue absorption peak or absorption band was detected.

In order to investigate the interface of the sample, the heterostructure $In_2O_3/In(OH)_3$ (sample c) was chosen for TEM. Fig. 6a gives an overview of the typical TEM image of the heterostructure $In_2O_3/In(OH)_3$. The cube with the mean size of 37 nm was $In_2O_3$. The rod like substance dispersing around the cubic $In_2O_3$ was $In(OH)_3$. Fig. 6b shows the high-resolution (HRTEM) image of $In_2O_3$.

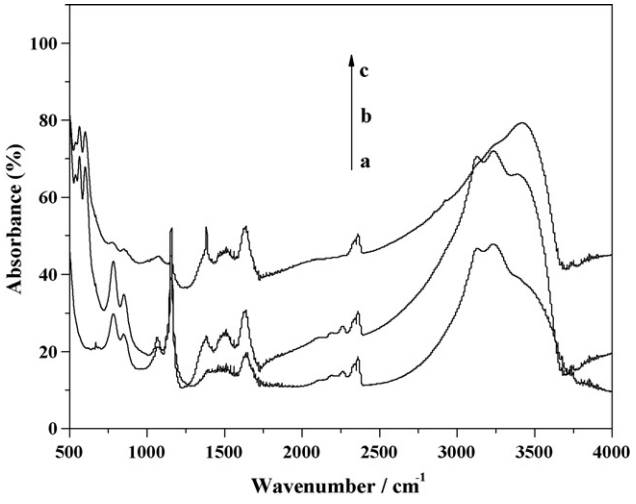


**Fig. 5.** FT-IR spectra of the samples. (a) $In(OH)_3$; (b) heterostructure $In_2O_3/In(OH)_3$; (c) $In_2O_3$.

Fig. 6c shows the patterns of the selected area electron diffraction of $In_2O_3$. It can be seen that the labeled rings correspond to diffraction of (2 2 2), (4 4 0) and (6 2 2) planes, respectively.

It is generally believed that the generation of free •OH radical is responsible for photocatalytic oxidation. More free •OH radicals imply stronger photocatalytic oxidation. Using terephthalic acid as a probe molecule by a photoluminescence (PL) technique to detect the formation of free •OH radicals has been a frequently used method in sonochemistry, biochemistry, and radiation chemistry [31,32]. Terephthalic acid readily reacts with •OH radicals to produce highly fluorescent product, 2-hydroxyterephthalic acid [19]. The intensity of the PL peak of 2-hydroxyterephtalic acid is in proportion to the amount of •OH radicals produced in water [33].

The fixed illumination time is 40 min. The PL spectra changes of the samples (a–e) excited at 315 nm in terephthalic acid solution were recorded, respectively, as is shown in Fig. 7. From Fig. 7, it is clear that the PL intensity of the heterostructure $In_2O_3/In(OH)_3$ (sample b) is the strongest, and the PL intensity of $In(OH)_3$ is higher than that of the $In_2O_3/In(OH)_3$ (samples c and d) and $In_2O_3$. It is proposed that more •OH radicals produced at the heterostructure $In_2O_3/In(OH)_3$ (sample b) surface than that of pure $In(OH)_3$ and other samples. The PL intensity of the heterostructure $In_2O_3/In(OH)_3$ decreases gradually with the increase in the amount of $In_2O_3$, and the PL intensity of $In_2O_3$ is the lowest. The result also showed that without the presence of the $In_2O_3/In(OH)_3$ and $In_2O_3$, no obvious emission spectrum was detected at 425 nm. Meanwhile, the PL intensity of the heterostructure $In_2O_3/In(OH)_3$ is stronger than that of $In_2O_3$, indicating more •OH radicals were produced at the heterostructure $In_2O_3/In(OH)_3$ surface than that of $In_2O_3$.

The photocatalytic activities of the samples were investigated by photocatalytic oxidation of rhodamine B. The dark absorption and blank tests were carried out simultaneously. The blank test shows that the photo-induced self-sensitized photodegradation has little influence on the results of experiment.

The fixed illumination time is 40 min. Fig. 8 shows the effect of the samples (a–e) on the photodegradation of rhodamine B (RhB) under UV light irradiation. From Fig. 8, it can be seen that the photocatalytic activity of the heterostructure $In_2O_3/In(OH)_3$ (sample b) is the highest and the photodegradation efficiency reaches up to 51.0%. The photocatalytic activity of $In(OH)_3$ is higher than that of the $In_2O_3/In(OH)_3$ (samples c and d) and $In_2O_3$, and the photocatalytic activity of the heterostructure $In_2O_3/In(OH)_3$ decreases gradually with the increase in the amount of $In_2O_3$. The result of the activity test is consistent with that of the hydroxyl radicals (•OH) experiment.

It is known that the photocatalytic activity of photocatalyst mainly depends on whether the electron–hole pairs can be separated effectively [16]. On the photocatalyst surface, the photoexcited electrons and holes can change in various ways. Among them, the two competitive processes, i.e., capture and recombination, are the most important ones. Photocatalytic reaction is effective only when the photoexcited electrons–holes can be captured. If there are no appropriate capturers of electrons or holes, they will recombine with each other and give off heat inside or on the surface of semiconductor. In order to increase the photocatalytic activity of photocatalyst, two important ways should be considered from the mechanism of the separation of photoexcited electrons and holes. One is to increase the separation efficiency of the photoexcited electron–hole pairs, and the other is to increase the amount of the photoexcited active species. For the heterostructure photocatalysts, two prerequisites for electron transfer are the electron density diversity and the energy gap of the heterostructure semiconductor materials [34]. Fig. 9 shows the band-gap structure diagram of $In(OH)_3$ and $In_2O_3$. The conduction band level of $In(OH)_3$ lies at about −0.8 eV (vs. NHE), while the valance band lies at about 4.37 eV. As for $In_2O_3$, the conduction band and valence band lie at

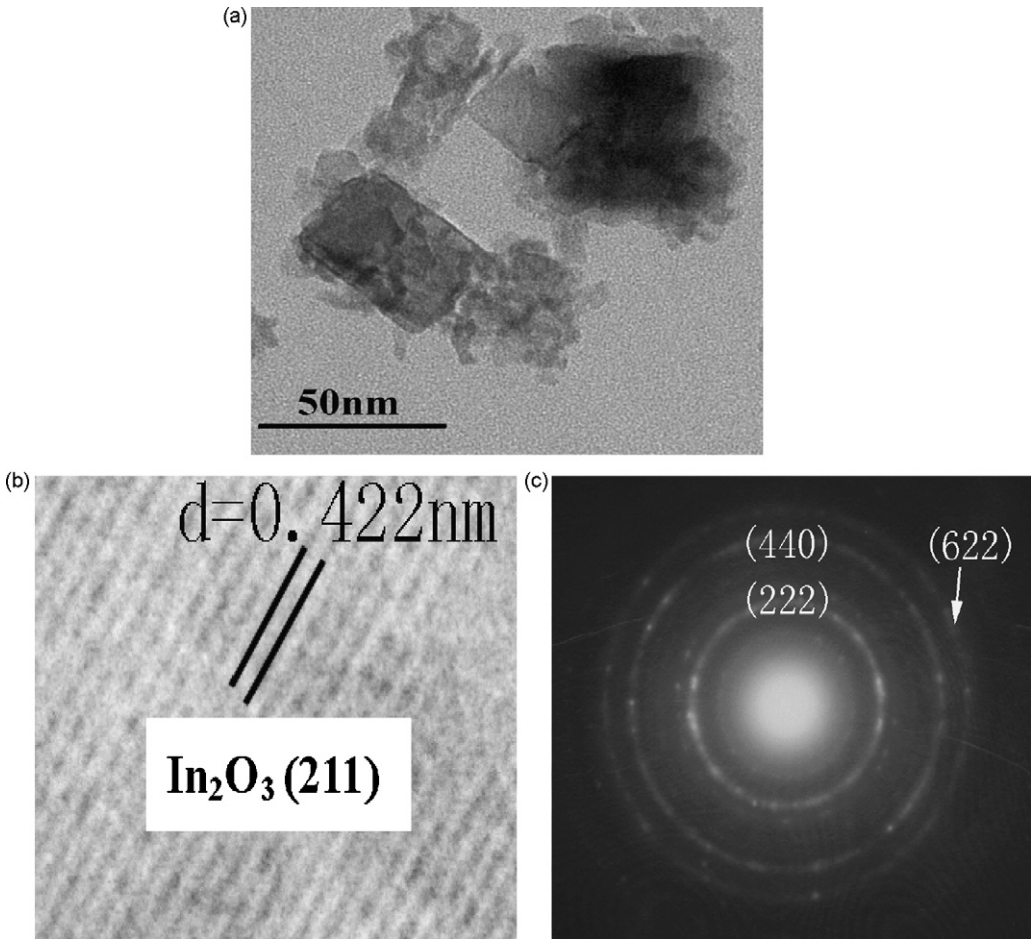


**Fig. 6.** TEM and HRTEM images of the heterostructure $In_2O_3/In(OH)_3$. (a) TEM image; (b) HRTEM image; (c) selected area electron diffraction pattern of $In_2O_3$.

about −0.509 eV and 2.071 eV, respectively. From Fig. 9, it can be seen that, when $In(OH)_3$ and $In_2O_3$ form a composite photocatalyst, it is unfavorable for the separation of photoexticed carriers. However, from Fig. 8, it is clear that the photocatalytic activity of the heterostructure $In_2O_3/In(OH)_3$ (sample b) is higher than that of single $In(OH)_3$ or $In_2O_3$. It may be attributed to the formation of heterostructure between $In_2O_3$ and $In(OH)_3$, which is favorable for the separation of photoexcited carriers and depresses the recombination of electron–hole pairs. Therefore, the photocatalytic activity is enhanced.

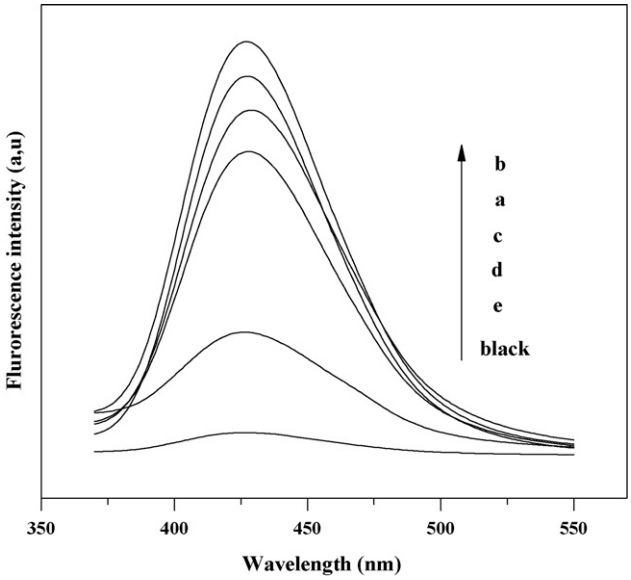


**Fig. 7.** PL spectra of the samples in terephthalic acid solution.

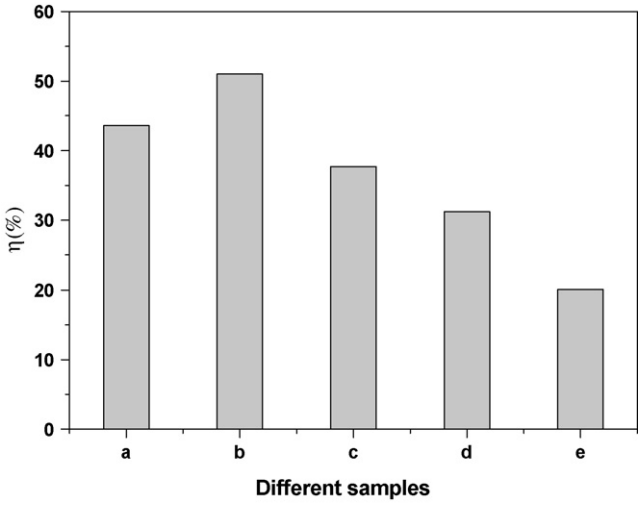


**Fig. 8.** Effect of the samples on the photodegradation of rhodamine B.

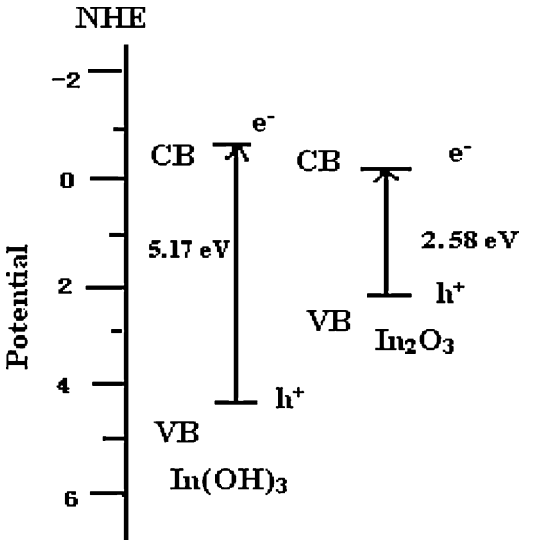


**Fig. 9.** Band-gap structure diagram of $In(OH)_3$ and $In_2O_3$.

## 4. Conclusion

Heterostructure $In_2O_3/In(OH)_3$ photocatalyst was prepared via programmed thermal treatment of $In(OH)_3$ precursor. The photocatalytic activity of the heterostructure $In_2O_3/In(OH)_3$ is higher than that of single $In(OH)_3$ or $In_2O_3$. The reason for the increased photocatalytic activity may be attributed to the formation of the heterojunction between $In_2O_3$ and $In(OH)_3$, which depresses the recombination of photoexcited electron–hole pairs.

## Acknowledgements

This work was supported by the Natural Science Foundation of China (Nos. 20673042, 20973071) and the Key Project of Science and Technology Research of Ministry of Education of China (208062).

## References

[1] J. Wang, M.S. Gudiksen, X. Duan, Y. Cui, C.M. Lieber, Highly polarized photoluminescence and photodetection from single indium phosphide nanowires, Science 293 (2001) 1455–1457.
[2] X. Duan, Y. Huang, R. Agarwal, C.M. Lieber, Single-nanowire electrically driven lasers, Nature 421 (2003) 241–245.
[3] W.S. Seo, H.H. Jo, K. Lee, B. Kim, S.J. Oh, J.T. Park, Size-dependent magnetic properties of colloidal $Mn_3O_4$ and MnO nanoparticles, Angew. Chem. Int. Ed. 43 (2004) 1115–1117.
[4] S.H. Sun, H. Zeng, Size-controlled synthesis of magnetite nanoparticles, J. Am. Chem. Soc. 124 (2002) 8204–8205.
[5] T. Hyeon, Chemical synthesis of magnetic nanoparticles, Chem. Commun. 8 (2003) 927–934.
[6] D. Zhang, C. Li, X. Liu, S. Han, T. Tang, C. Zhou, Doping dependent $NH_3$ sensing of indium oxide nanowires, Appl. Phys. Lett. 83 (2003) 1845–1847.
[7] R.G. Gordon, Criteria for choosing transparent conductors, MRS Bull. 25 (2000) 52–57.
[8] I. Hamberg, C.G. Granqvist, Evaporated Sn-doped $In_2O_3$ films: basic optical properties and applications to energy-efficient windows, J. Appl. Phys. 60 (1986) R123–R159.
[9] H.Q. Cao, X.Q. Qiu, Y. Liang, Q.M. Zhu, Room-temperature ultraviolet-emitting $In_2O_3$ nanowires, Appl. Phys. Lett. 83 (2003) 761–763.
[10] C.H. Lee, M. Kim, T. Kim, A. Kim, J. Paek, J.W. Lee, S.Y. Choi, K. Kim, J.B. Park, K. Lee, Ambient pressure syntheses of size-controlled corundum-type $In_2O_3$ nanocubes, J. Am. Chem. Soc. 128 (2006) 9326–9327.
[11] S. Avivi, A. Mastai, Gedanken, Sonohydrolysis of $In^{3+}$ ions: formation of needlelike particles of indium hydroxide, Chem. Mater. 12 (2000) 1229–1233.
[12] Z.H. Li, T.T. Dong, Y.F. Zhang, L. Wu, J.Q. Li, X.X. Wang, X.Z. Fu, Studies on $In(OH)_yS_z$ solid solutions: syntheses, characterizations, electronic structure, and visible-light-driven photocatalytic activities, J. Phys. Chem. C 111 (2007) 4727–4733.
[13] Z.B. Lei, G.J. Ma, M.Y. Liu, W.S. You, H.J. Yan, G.P. Wu, T. Takata, M. Hara, K. Domen, C. Li, Studies on $In(OH)_yS_z$ solid solutions: syntheses, characterizations, electronic structure, and visible-light-driven photocatalytic activities, J. Catal. 237 (2006) 322–329.
[14] S.F. Chen, W. Zhao, W. Liu, S.J. Zhang, Preparation characterization and activity evaluation of p–n junction photocatalyst p-ZnO/n-$TiO_2$, Appl. Surf. Sci. 255 (2008) 2478–2484.
[15] S.F. Chen, L. Chen, S. Gao, G.Y. Cao, The preparation of coupled $WO_3/TiO_2$ photocatalyst by ball milling, Powder Technol. 160 (2005) 198–202.
[16] S.F. Chen, S.J. Zhang, W. Liu, W. Zhao, Preparation and activity evaluation of p–n junction photocatalyst NiO/$TiO_2$, J. Hazard. Mater. 155 (2008) 320–326.
[17] W. Liu, S.F. Chen, S.J. Zhang, W. Zhao, H.Y. Zhang, X.L. Yu, Preparation and characterization of p–n heterojunction photocatalyst p-$CuBi_2O_4$/n-$TiO_2$ with high photocatalytic activity under visible and UV light irradiation, J. Nanopart. Res. 12 (2010) 1355–1366.
[18] Z.Y. Wang, B.B. Huang, Y. Dai, X.Y. Qin, X.Y. Zhang, P. Wang, H.X. Liu, J.X. Yu, Highly photocatalytic ZnO/$In_2O_3$ heteronanostructures synthesized by a coprecipitation method, J. Phys. Chem. C 113 (2009) 4612–4617.
[19] K. Ishibashi, A. Fujishima, T. Watanabe, K. Hashimoto, Detection of active oxidative species in $TiO_2$ photocatalysis using the fluorescence technique, Electrochem. Commun. 2 (2000) 207–210.
[20] J.G. Yu, W.G. Wang, B. Cheng, B.L. Su, Enhancement of photocatalytic activity of mesoporous $TiO_2$ powders by hydrothermal surface fluorination treatment, J. Phys. Chem. C 113 (2009) 6743–6750.
[21] L.C. Schumacher, S. Mamiche-Afara, M. Leibovitch, M.J. Dignam, Achieving high-efficiency photoanodic behavior with a low-mobility oxide $In_2O_3$, J. Electrochem. Soc. 135 (1988) 3044–3050.
[22] R.L. Weiher, R.P. Ley, Optical properties of indium oxide, J. Appl. Phys. 37 (1966) 299–302.
[23] V. Damodara Das, S. Kirupavathy, L. Damodare, N. Lakshminarayan, Optical and electrical investigations of indium oxide thin films prepared by thermal oxidation of indium thin films, J. Appl. Phys. 79 (1996) 8521–8530.
[24] Y. Ohhata, F. Shinoki, S. Yoshida, Optical properties of reactive sputtered tin-doped $In_2O_3$ films, Thin Solid Films 59 (1979) 255–261.
[25] A. Raza, O.P. Agnihotri, B.K. Gupta, Preparation and intrinsic absorption in the band edge in chemically sprayed $In_2O_3$ layers, J. Phys. D: Appl. Phys. 10 (1977) 1871–1876.
[26] Y.P. Sun, C.J. Murphy, K.R. Reyes-Gil, E.A. Reyes-Garcia, J.P. Lilly, D. Raftery, Carbon-doped $In_2O_3$ films for photoelectrochemical hydrogen production, Electrochim. Acta 45 (2000) 1595–1605.
[27] A. Walsh, J.L.F. Da Silva, S.H. Wei, C. Korber, A. Klein, L.F.J. Piper, A. DeMasi, K.E. Smith, G. Panaccione, P. Torelli, D.J. Payne, A. Bourlange, R.G. Egdell, Nature of the band gap of $In_2O_3$ revealed by first-principles calculations and X-ray spectroscopy, Phys. Rev. Lett. 100 (2008) 167402–167406.
[28] A.N. Christensen, N.C. Broch, O.V. Heidenstam, A. Nilsson, Hydrothermal investigation of the systems $In_2O_3$–$H_2O$–$Na_2O$ and $In_2O_3$–$D_2O$–$Na_2O$. The crystal structure of rhombohedral $In_2O_3$ and of $In(OH)_3$, Acta Chem. Scand. 21 (1967) 1046–1056.
[29] Y.S. Chen, X.X. Wang, D.Z. Li, X.Z. Fu, Preparation and characterization of $In(OH)_3$ nanocrystal with high photocatalytic activity and stability, Chem. J. Chin. Univ. 28 (2007) 355–357.
[30] W.B. White, V.G. Keramidas, Vibrational spectra of oxides with the c-type rare earth oxide structure, Spectrochim. Acta 28A (1972) 501–509.
[31] S.C. Ashawa, U.R. Kini, U. Madhvanath, The aqueous coumarin system as a low range chemical dosimeter, Int. J. Appl. Radiat. Isot. 30 (1979) 7–10.
[32] X.W. Fang, G. Mark, C.V. Sonntag, OH radical formation by ultrasound in aqueous solutions. Part I. The chemistry underlying the terephthalate dosimeter, Ultrason. Sonochem. 3 (1996) 57–63.
[33] Y.H. He, D.Z. Li, G.C. Xiao, W. Chen, Y.B. Chen, M. Sun, H.J. Huang, X.Z. Fu, A new application of nanocrystal InS in efficient degradation of organic pollutant under visible light irradiation, J. Phys. Chem. C 113 (2009) 5254–5262.
[34] S.M. Sze, K.N. Kwok, Physics of Semiconductor Devices, 3rd ed., Wiley, New York, 2007.